Solid State Ionics 273 (2015) 46–50

Contents lists available at ScienceDirect

Solid State Ionics

journal homepage: www.elsevier.com/locate/ssi

First principles modeling of Ag adsorption on the $LaMnO_3$ (001) surfaces

A.U. Abuova [a,*], Yu.A. Mastrikov [b], E.A. Kotomin [b], Y. Kawazoe [c,d], T.M. Inerbaev [a], A.T. Akilbekov [a]

[a] L.N. Gumilyov Eurasian National University,Mirzoyan str. 2, Astana, Kazakhstan
[b] Institute of Solid State Physics, University of Latvia, Kengaraga str. 8, Riga, Latvia
[c] New Industry Creation Hatchery Center, Tohoku University, 6-6-4 Aramaki-aza-Aoba, Aobaku, Japan
[d] Institute of Thermophysics, Siberian Branch of the Russian Academy of Sciences, 1, Lavyrentyev Avenue, Novosibirsk 630090, Russia

ARTICLE INFO

Article history:
Received 22 June 2014
Received in revised form 28 September 2014
Accepted 30 September 2014
Available online 16 October 2014

Keywords:
$LaMnO_3$
Surface
Ag adsorption
Solid oxide fuel cells
Ab initio calculations

ABSTRACT

Doping of oxide surfaces with Ag atoms could improve their catalytic properties, e.g. for solid oxide fuel cell and oxygen permeation membrane applications. We present results of the ab initio calculations of Ag adsorption on the $LaMnO_3$ (LMO) (001) surfaces. The energetically most favorable adsorption sites for low coverage of Ag atoms and monolayer on both MnO_2- and LaO-terminations have been determined. The electron charge transfer between Ag and substrate and interatomic distances have been analyzed. The Ag atom migration along the MnO_2 surface is ~0.5 eV which could lead to a fast clustering of adsorbates at moderate temperatures whereas the adhesion energy of silver monolayer is relatively low which could indicate its mechanical instability.

1. Introduction

Solid oxide fuel cells (SOFCs) are of a great technological interest as they offer high efficiency for energy conversion in a clean way [1]. This interest in SOFC technology is driven by their potential for high efficiency energy conversion with reduced emission of greenhouse gases compared to other more conventional power generation routes [2,3] and is also used in combined heat and power applications [4,5].

Different methods have been used to prepare functionalized composite cathodes with improved electrochemical performance and long term stability at reduced operating temperature [6]. In particular, metallic silver is a potential component for the SOFC cathode operated below 800 °C as well as oxygen permeation membranes (OPM) because of its good catalytic activity, high electrical conductivity, and relatively low cost. However, even far below its melting point, silver atoms are mobile and (describe the problem: form clusters and/or move out from the cathode or something else). Therefore, silver dopant properties should be addressed prior to a long-term application of silver-based cathodes in SOFC or permeation membranes.

Recently, $(La_{0.8}Sr_{0.2})_{0.95}Ag_{0.05}MnO_{3-\delta}$ was suggested as a high performance intermediate temperature cathode material, in which Ag serves as an effective catalyst through an intercalation/deintercalation mechanism [7]. Under cathodic polarization, Ag moves out of cathode to be deposited in a form of small nanoclusters, leaving the remaining $(La_{0.8}Sr_{0.2})_{0.95}MnO_{3-\delta}$ (LSM) as a catalyst carrier. The Ag nanoclusters with size of 5–15 nm are very active and stable in catalyzing the cathode reaction even at reduced temperatures. Under anodic polarization, the Ag moves back into the deficient sites of the LSM. This could permit a regeneration method to restore Ag nanoclusters, which may otherwise become degraded over time by fusing together, thereby losing the activity. According to recent experiments [8–10], Ag/LMO system has also been reported to be a prominent catalyst for the oxygen reduction reaction in SOFC applications. Elucidating the mechanisms of oxygen reduction on Ag/LMO (001) surfaces is beneficial for understanding the limitations of the currently used materials in SOFC technology and supporting the development of higher performance materials [11].

However, the Ag/LMO system is poorly studied compared with e.g. Ag/CeO_2. We are familiar with the only theoretical investigation on the silver and oxygen adsorption on the LMO (001) surfaces [11]. This study has, however, serious limitations: the supercell is assumed cubic and is quite small so the defect density is unrealistically large (per surface unit cell 0.5 atom Ag), and only one surface termination was considered. In this paper, we discuss adsorption mechanisms on Ag/LMO (001) catalyst surfaces using first-principles Density Functional Theory (DFT)-based calculations on. As the first step, the electronic properties and interaction between Ag atom and LaO and MnO_2-terminated surfaces are studied here, in order to study silver effects on oxygen reduction reaction in the next paper. For the energetically most favorable structures of catalyst/cathode material solid solutions the analysis of local structure around catalyst atoms will be carried out, in order to recognize

* Corresponding author.

http://dx.doi.org/10.1016/j.ssi.2014.09.039
0167-2738/

Table 1
Optimization of lattice constants (Å) with fixed experimental positions of atoms inside the orthorhombic unit cell of 40 atoms. E_{coh} — cohesive energies for four different magnetic orderings.

	a, Å	*b*, Å	*c*, Å	E_{coh} (eV/cell)
Expt [21]	5.7473	7.6929	5.5367	30.3
FM	5.7787	7.7349	5.5669	31.80
A-AF	5.7724	7.7265	5.5618	31.82
C-AF	5.7683	7.7210	5.5569	31.78
G-AF	5.7734	7.7278	5.5609	31.79

possible migration pathway along the surface and the Ag diffusion barrier.

2. Computational details

Periodic DFT calculations were performed using the program VASP 5.3.3 [12] with Projector Augmented Wave (PAW) pseudopotentials and the exchange–correlation PBE functional of the GGA-type [12,13]. We tested preliminarily [14] three types of PAW pseudopotentials for the inner electrons—La, Mn_*pv*, O, where the lower index *pv* means that *p* states are treated as valence states and *s* stands for soft pseudopotentials with reduced cutoff energy and/or reduced number of electrons. As a result, we used a set of pseudopotentials, which provides a good combination of computational resources and accuracy [15,16]. In our test calculations we compared LMO rhombohedral and (experimentally observed) orthorhombic phases and different values of the cutoff energy. After these tests, we implemented orthorhombic phase for the further calculations, and used the kinetic energy cutoff at 520 eV. For the surface calculations the Brillouin zone was sampled with the $4 \times 4 \times 1$ Monkhorst–Pack scheme [13]. Since the difference in energy between the different magnetic states is much less than those of the process under study, we used ferromagnetic (FM) state in all our surface calculations, as the most stable one [17].

To study the magnetic ordering in LMO, the so-called broken symmetry approach was adopted [18]. It allows us to deduce the magnitude of the magnetic coupling data making spin-polarized calculations for different magnetic orderings of transition metal atoms. LMO bulk crystal at moderate temperatures reveals the orthorhombic structure comprising four formula units, with the space group 62 (in P*bnm* and P*nma* settings the largest orthorhombic lattice translation vector is directed along the *z* or *y* axis, respectively; in this paper, the P*bnm* setting is chosen). The effective atomic charges are calculated using the Bader (topological) analysis [19,20].

In our surface model, we used a slab infinite in two (*x*, *y*) dimensions and containing a finite number of planes along the *z* axis normal to the surface. The orthorhombic surface unit cell has an area twice as large as for the cubic unit cell. A large vacuum gap of 19.8 Å between slabs periodically repeated along the *z* axis was used, in order to prevent

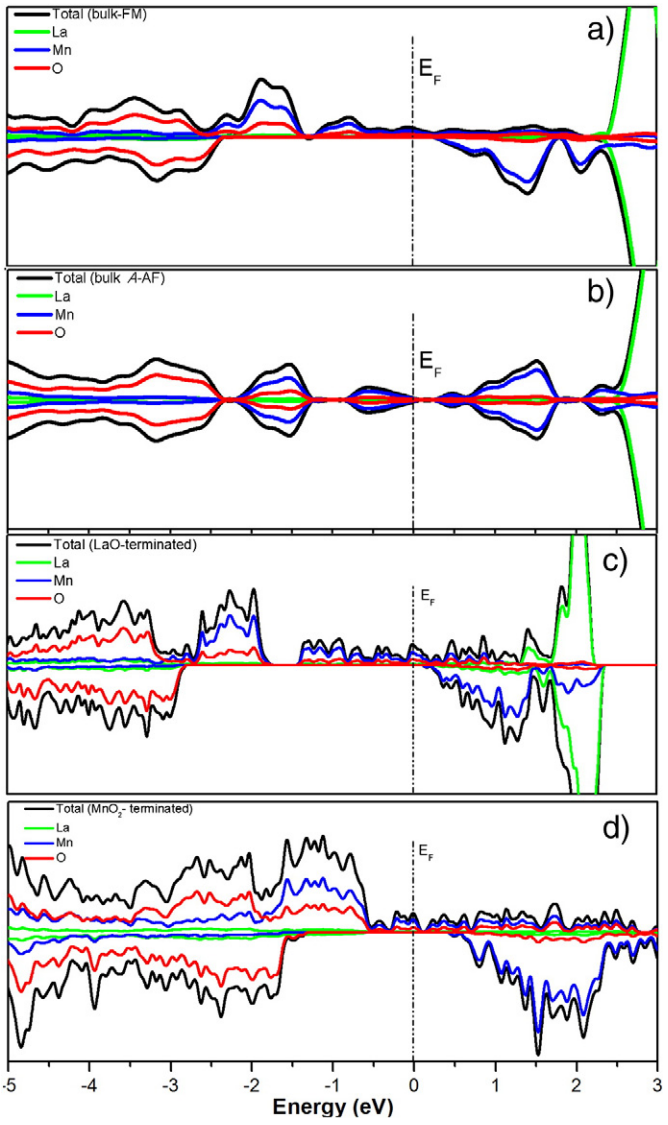

Fig. 1. DOS of the perfect LMO: a) perfect FM bulk, b) *A*-AF bulk, c) LaO-termination, and d) MnO_2-termination surfaces. The Fermi energy is taken as zero.

an interaction between the two surfaces through the vacuum region. The structure optimization performed with surface Ag concentration, which varied between 1 atom Ag until monolayer per 8 surface unit cells. The adsorption energy is calculation according to the equation:

$$E_{ads} = E_{[Ag/slab]} - E_{[Ag]} - E_{[slab]}, \quad (1)$$

Table 2
Optimization of lattice constants (Å) orthorhombic and rhombohedral unit cell of 40 atoms. E_{coh} — cohesive energies for four different magnetic orderings. The numbers in bracket are the experimental data for orthorhombic [21] and rhombohedral [25] phases. Atomic coordinates in the supercells were also optimized.

	Orthorhombic phase				Rhombohedral phase		
	a, Å (5.7473)	*b*, Å (7.6929)	*c*, Å (5.5367)	E_{coh} (eV/cell) (30.3)	*a*, Å (5.5285)	*c*, Å (13.3348)	E_{coh} (eV/cell)
FM	5.6304	7.8649	5.5496	31.84	5.4786	13.3956	31.76
A-AF	5.8718	7.6575	5.5565	31.65	5.5102	13.3317	31.65
C-AF	5.9334	7.6864	5.5231	31.12	5.5521	13.3624	31.53
G-AF	5.6765	7.6756	5.6944	30.70	5.5376	13.3754	31.40

where $E_{[Ag/slab]}$ and $E_{[slab]}$ are the calculated total electronic energies of the adsorbed silver species on the surface and a clean surface. The adsorption energy is a criterion to determine the stability of Ag atoms and to estimate their surface mobility. The binding energy of Ag monolayer was calculated as the difference of the total energies of bound and separate systems.

3. Results and discussion

The orthorhombic bulk lattice constant calculations were first performed and compared with the previous calculations and experimental value [11,14,17,21], which confirm that the chosen calculation parameters give realistic results. Table 1 presents three optimized lattice parameters of the low-temperature orthorhombic phase and the cohesive energies for four different magnetic orderings. Depending on the four Mn spin orientations in the orthorhombic unit cells of 40 atoms, there are four possible magnetic orderings: ferromagnetic (FM, all spins are parallel), as well as *A*-, *G*-, and *C*-type antiferromagnetic (*A*-AF, *G*-AF, and *C*-AF). In the *A*-AF case the Mn spins are parallel in basal plane and antiparallel from plane to plane; in the *G*-AF each nearest neighbor pair of Mn spins is antiparallel, and in the *C*-AF each nearest neighbor pair of Mn spins is antiparallel in the basal plane and parallel along the *z* axis. The cohesive energies were calculated as the difference of the VASP unit cell total energy and the sum of the atomic energies of the constituent atoms. The atomic coordinates in the unit cell were fixed according to the experimental data [21]. In agreement with the experiment, the lowest energy corresponds to the *A*-AF structure.

Table 2 presents the optimized lattice parameters of the orthorhombic and possible rhombohedral phase and the cohesive energies for four above-mentioned different magnetic orderings. Along with lattice constants, the atomic coordinates in the supercells were also optimized. The FM state in orthorhombic cell is energetically more favorable than that in the rhombohedral one, whereas the *A*-AF energies in both phases reveal the same energies. In contrast to the experimentally observed ground state, the *A*-AF structure in our calculations is slightly higher in energy than FM structure [22,23].

We calculated also the density of states (DOS) for the perfect ferromagnetic (FM) and anti-ferromagnetic (*A*-AF) bulk, as well as defect-free LaO-and MnO_2-terminated slabs (Fig. 1). As one can see here, in agreement with experiments, only in *A*-AF state LMO has a non-zero gap (0.5 eV). Also in agreement with previous studies, the valence band is a mixture of O 2*p* states with Mn 3*d* states, which form also the conduction band bottom, whereas La states lie at higher energies. Based in these results, one can conclude that the GGA approximation could reproduce basic experimental results on the LMO bulk and thus will be used in this paper.

Note that as was shown earlier [24], MnO_2-terminated surface is energetically more favorable than LaO-one under normal operational condition.

3.1. Ag atom adsorption on the LaO terminated (001) surface

Full slab geometry optimization was performed. For Ag adsorption, we considered two possible sites on LaO (001) surface: "hollow-1" and "hollow-2" positions (Fig. 2a and Table 3). The calculated adsorption energies are 2.03 eV and 1.76 eV, respectively. The effective atomic (Bader) charges in Table 3 show that La ions have a charge close to $+2e$, instead of a formal charge $+3e$, whereas O also has a charge much smaller than a formal $-2e$. This demonstrates considerable covalency of the LMO chemical bonding. There is also considerable charge transfer from substrate towards Ag adatoms which are negatively charged.

For further understanding the effect of Ag adsorption on the electronic structure of LaO (001) surface, we have calculated the DOS for a defect-free surfaces, before Ag adsorption (Fig. 1c), and Projected DOS (PDOS) after Ag adsorption—with coverage of one Ag atom per 8 surface unit cells (Fig. 3a) and 2 Ag atoms per 1 surface unit cell (monolayer) (Fig. 3b). The Ag states overlap strongly with the valence band, which explains observed charge transfer from O 2*p* to adsorbed Ag atoms. The PDOS for Ag monolayer reflects formation of the metallic band.

3.2. Ag atom adsorption on the MnO_2-terminated (001) surfaces

The energetically most stable position of the adsorbed Ag atom is a "bridge O–O" site — see Fig. 2b and Table 4 where the effective atomic charges are also listed. The hollow position is very close in energy. Note that Ag gets a considerable charge transfer (0.56 e) from adsorbate only at the hollow position, whereas both Mn and O charges indicate a considerable covalency of their chemical bonds.

To further understand the effect of the Ag adsorption on the electronic structure of MnO_2 (001) surface, we also calculated DOS

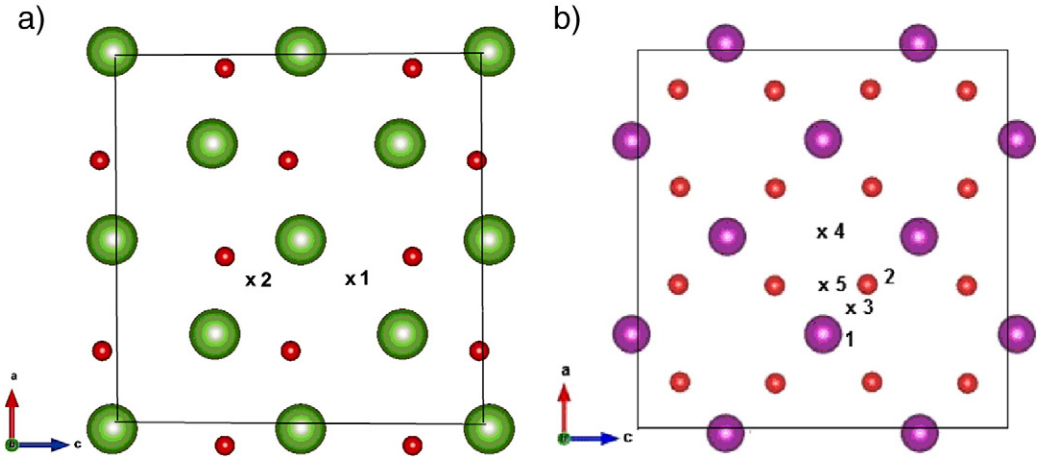

Fig. 2. Atomic Ag adsorption on the $LaMnO_3$ (001) surface a) stable adsorption sites on the LaO-terminated: 1—"hollow-1" position and 2—"hollow-2" position. b) Stable adsorption sites on the MnO_2-terminated: 1—atop Mn, 2—atop O, 3—"bridge Mn–O" position, 4—"hollow" position, and 5—"bridge O–O" position. Green, purple, and red balls denote La, Mn, and O ions, respectively.

Table 3
Calculated adsorption properties for Ag atom on the LaO-terminated (001) surface.

Ads. Site	E_{ads}, eV	Distance, Å		Charge, *e*		
		Ag–O	Ag–La	Ag	O	La
"Hollow-1"	2.03	3.48	3.35	−0.69	−1.29	1.97
"Hollow-2"	1.76	3.33	3.34	−0.68	−1.29	1.91
Monolayer	0.31	3.58	3.01	−0.78	−1.54	1.85

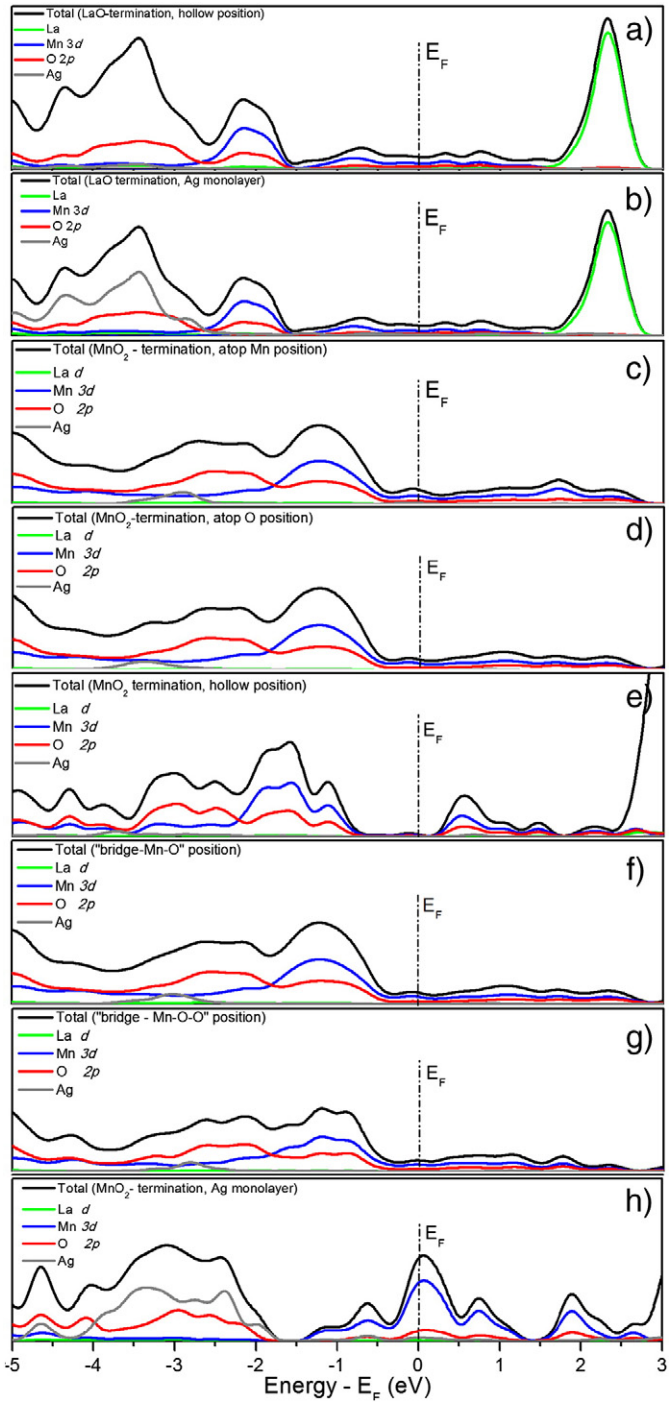

Fig. 3. PDOS of the adsorption Ag atoms (1 atom Ag per 8 surface unit cells): a) LaO-termination, "hollow" position, b) Ag monolayer (per surface unit cell 2 atom Ag) on the LaO termination, c) atop Mn, d) atop O, e) "hollow" position, f) "bridge Mn–O" position, g) "bridge O–O" position on the MnO_2 termination, and h) Ag monolayer (per surface unit cell 2 atom Ag) on the MnO_2 termination.

Table 4
Calculated adsorption properties for Ag atom on MnO_2-terminated (001) surface. The numbers in brackets are calculations [11] for per surface unit cell 0.5 atom Ag coverage.

Ads. site	E_{ads}, eV	Distance, Å		Charge, *e*		
		Ag–O	Ag–Mn	Ag	O	Mn
Atop Mn	1.10 (1.72)	3.38	2.59	0.01	−1.16	1.59
Atop O	1.03 (1.80)	2.50	2.87	0.08	−1.17	1.61
"Bridge Mn–O"	1.04	2.86	2.62	0.04	−1.18	1.58
"Hollow"	1.60	2.37	3.11	0.57	−1.16	1.65
"Bridge-O–O"	1.65 (2.10)	2.65	2.79	0.56 (−0.33)	−1.18	1.57
Monolayer	0.88	3.24	2.98	0.01	−0.98	1.65

before Ag adsorption surface (Fig. 1d), and PDOS after Ag adsorption surface (Fig. 3c–h). Both defect-free and adsorbed MnO_2 surfaces are metallic, with Ag peak overlapping the O 2*p* valence band.

3.3. Silver monolayer adsorption

We calculated also the energy of Ag monolayer adsorption on the LaO surface (Fig. 4a), which is quite low, about 0.3 eV per atom (Table 3). This is much smaller than the adsorption energy for single Ag atoms because in metal layer the strongest interaction occurs between Ag atoms rather between Ag and adsorbate. This is a reason why Ag monolayer could be mechanically unstable and easily removed from the LMO surface.

Ag monolayer adsorption on the MnO_2-terminated surface (Fig. 4b) was modeled by placing atoms at two possible sites: hollow and Mn. After atomic optimization Ag atoms shifted from the initial positions as shown in Fig. 4. The adorption energy of Ag monolayer turned out to be 0.88 eV per atom (Table 4), smaller than for a single Ag atom but larger than for Ag monolayer on LaO surface.

4. Conclusions

1. The energetically most favorable positions for Ag atom adsorption on both the LaO- and MnO_2-terminated orthorhombic (001) $LaMnO_3$ surfaces are hollow and bridge O–O sites, respectively with the binding energies 2.03 eV and 1.65 eV, respectively.
2. The Ag migration energy on the MnO_2 surface is quite low, ca. 0.5 eV which allows easy silver clusterization.
3. A small cohesive energy of Ag monolayer has been observed on both the LaO- and the MnO_2-terminated surfaces. On the LaO-terminated surface Ag atoms occupy hollow positions with the energy 0.31 eV per single Ag atom. On the MnO_2-terminated surface Ag atoms are located close to Mn and hollow sites, slightly shifted from them along the same direction. For this termination, adsorption energy is slightly higher, 0.88 eV per single Ag atom. The obtained energies show that Ag monolayer could be easily removed from the (001) LMO surface.

Acknowledgments

This study was partly supported by the EC GREEN-CC project (grant agreement 608524), the Latvian Research grant 237/2012 and the grant of Kazakhstan 137/2013. Y. M. thanks ESF project nr. 2013/0015/1DP/1.1.1.2.0/13/APIA/VIAA/010. Authors are indebted to J. Serra and R. Merkle for stimulating discussions. One of the authors (Y. K.) thanks the Russian Mega Grant project no. 14.B25.31.0030 "New energy technologies and energy carriers" for supporting the present research.

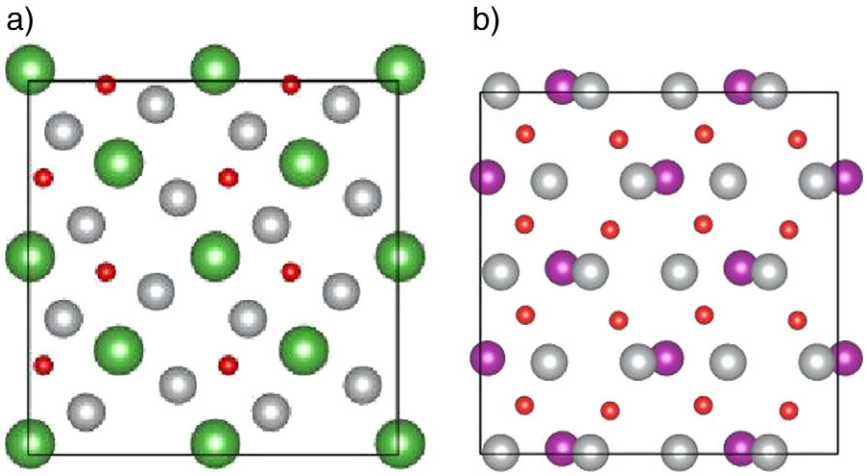

Fig. 4. Adsorption of Ag monolayer on the (001) $LaMnO_3$ surface: a) LaO-terminated and b) MnO_2-terminated. Green, purple, red, and gray balls denote La, Mn, O, and Ag ions, respectively.

References

[1] M. Kuklja, E.A. Kotomin, R. Merkle, Yu. Mastrikov, J. Maier, Phys. Chem. Chem. Phys. 15 (2013) 5443–5471.
[2] S.C. Singhal, Solid State Ionics 135 (2000) 305–313.
[3] B.C.H. Steele, A. Heinzel, Nature 414 (2001) 345–352.
[4] A.J. Jacobson, Chem. Mater. 22 (2010) 660–674.
[5] J. Fleig, Annu. Rev. Mater. Res. 33 (2003) 361–382.
[6] S. Huang, S. Feng, H. Wang, Y. Li, C. Wang, Int. J. Hydrogen Energy 36 (2011) 10968–10974.
[7] W. Zhou, Z. Shao, F. Liang, Z.-G. Chen, Z. Zhu, W. Jin, N. Xu, J. Mater. Chem. 21 (2012) 15343–15351.
[8] V.A.C. Haanappel, D. Rutenbeck, A. Mai, S. Uhlenbruck, D. Sebold, H. Wesemeyer, B. Rowekamp, C. Tropartz, F. Tietz, J. Power Sources 130 (2004) 119.
[9] S. Uhlenbruck, F. Tietz, V.A.C. Haanappel, D. Sebold, J. Solid State Electrochem. 8 (2004) 923.
[10] W. Wang, H. Zhang, G. Lin, Z. Xiong, Appl. Catal. B 24 (2000) 219.
[11] Y. Zhou, Z. Lu, B. Wei, X. Zhu, X. Huang, W. Jiang, W. Su, J. Power Sources 209 (2012) 158–162;
Y. Zhou, Z. Lu, P. Guo, Ya Tian, X. Huang, W. Su, Appl. Surf. Sci. 258 (2012) 2602–2606.
[12] G. Kresse, J. Hafner, VASP the Guide, University of Vienna, 2007. (http://cms.mpi.univie.ac.at/vasp/);
G. Kresse, J. Hafner, Phys. Rev. B 47 (1993) 558–561;
G. Kresse, J. Furthmueller, Phys. Rev. B 54 (1996) 11169–11186.
[13] J.P. Perdew, K. Burke, M. Ernzerhof, Phys. Rev. Lett. 77 (1996) 3865.
[14] E.A. Kotomin, R.A. Evarestov, Yu.A. Mastrikov, J. Maier, Phys. Chem. Chem. Phys. 7 (2005) 2346.
[15] S. Piskunov, E.A. Kotomin, E. Heifets, J. Maier, R.I. Eglitis, G. Borstel, Surf. Sci. 75 (2005) 575.
[16] R.A. Evarestov, E.A. Kotomin, Yu.A. Mastrikov, D. Gryaznov, E. Heifets, J. Maier, Phys. Rev. B 72 (2005) 214411.
[17] E.A. Kotomin, Y.A. Mastrikov, E. Heifets, J. Maier, Phys. Chem. Chem. Phys. 10 (2008) 4644.
[18] Y.A. Mastrikov, R. Merkle, E. Heifets, E.A. Kotomin, J. Maier, J. Phys. Chem. C 114 (2010) 3017.
[19] D. Munoz, N.M. Harrison, F. Illas, Phys. Rev. B 69 (2004) 085115.
[20] G. Henkelman, A. Arnaldsson, H. Jónsson, Comput. Mater. Sci. 36 (2006) 354.
[21] J.R. Carvajal, M. Hennion, F. Moussa, A.H. Moudden, Phys. Rev. B 57 (1998) 3190.
[22] Y.-S. Su, T.A. Kaplan, S.D. Mahanti, J.F. Harrison, Phys. Rev. B 61 (2000) 1324.
[23] M. Nicastro, C.H. Patterson, Phys. Rev. B 65 (2002) 205111.
[24] E. Heifets, E.A. Kotomin, Yu A. Mastrikov, S. Piskunov, J. Maier, Thermodynamics — Interaction Studies — Solids, Liquids and GasesChapter in a book: InTech Open Access Publishers, 2011. 491–518.
[25] Q. Huang, A. Santoro, J.W. Lynn, R.W. Erwin, J.A. Borchers, J.L. Peng, R.L. Greene, Phys. Rev. B 55 (14) (1997) 987.